The Spatial Mapping of Interconversion Between Laguerre-Gaussian and Hermite-Gaussian Beams Array With an Astigmatism Phase

Ao Tang , Guangyun Xiong, Lan Bin, and Feng Shen

Abstract—**The Laguerre-Gaussian (LG) and Hermite-Gaussian (HG) modes can be interconverted with an astigmatism phase. In this paper, based on the single beam, the interconversion of LG and HG beams array with the astigmatism phase is analyzed theoretically and the spatial mapping relationship is derived. In the experiment, 1×3, 2×2, 3×3 LG beams arrays are generated and converted into HG beams array via employing a spatial light modulator loaded with $0°$, $90°$, $45°$, $-45°$ astigmatism phases. The experimental results are in great agreement with the theoretical analyses. Moreover, from the number and direction of the dark fringe of converted HG beams array, the orbital angular momentum information of LG beams array can be obtained. This work theoretically perfects the theoretical model of the interconversion between LG and HG beams based on an astigmatism phase, and also provides a theoretical support for measuring the LG beams array.**

Index Terms—**Astigmatism phase, mode converter, orbital angular momentum, LG beams array.**

I. INTRODUCTION

THE Laguerre-Gaussian (LG) beam was demonstrated that carry orbital momentum angular (OAM) of $l\hbar$ per photon [1], where l is the topological charge, and $\hbar$ is the reduced Planck constant. Besides, the optical field is distributed in a annular shape, and the phase is the spiral structure with a phase singularity in the center, which is also called the vortex beam. Due to these unique characteristics, vortex beams have been intensively researched and applied in various fields. Especially in optical communications [2], where OAM as a new dimension of light, can increase channel capacity. Recently, multi-vortex geometric beams [3] and six-dimensional optical OAM multiplexing [4]

are proposed, which will greatly improve the performance of the OAM communication systems. Additionally, in the field of optical tweezers, it is possible to capture particles, and transfer the OAM to particles, then rotate them [5]. Due to its unique intensity distribution, it can also be employed in optical processing [6]. These applications rely on OAM, hence, measuring the OAM is a task of great significance.

The OAM of the light is generally characterized by detecting the magnitude and sign of the l, and many methods have been proposed, such as interference methods [7], [8], [9], [10] and diffraction methods [11], [12], [13]. Most of the interference methods require a reference beam, and diffraction methods usually require special optical element and strict beam alignment. Moreover, deep learning [14], surface plasmon [15] and spatial mode decompostion [16], [17] are also put forward. Recently, a cross phase was employed to detect OAM [18], which is an astigmatism phase that can achieve interconversion between the LG modes and Hermite Gaussian (HG) modes [19], and the intensity rotations of optical field is also investigated in conversion process [20], [21]. Zhibing Liu et al. detected the vortex beam up to 100-order by employing this phase [22]. Furthermore, Yujia Wu and Yongqiang Yang extended this method to detect the OAM of the near-infrared optical vortex [23] and terahertz optical vortex [24], respectively. However, the conversion of the beams array is not analyzed in these reports. Additionally, since muti-channel OAM beam can greatly improve the communication capacity, and in the field of optical tweezers, multiple particles can be captured simultaneously, thus, vortex beams array generation has also been researched [25]. However, there is currently no a good method to detect vortex beams array modes, most methods for measuring single-beam vortex beams require strict beam alignment, and measurement results will be distorted for off-center beams [26]. Therefore, a superior method for detecting vortex beams array is required, which allows for more efficient application of the vortex beams array in various fields.

In our investigation, the astigmatism phase is found to be insensitive to the position of the incident LG beam. For a LG beam incident at any position, it can be converted to a high-quality HG beam. This fact was also mentioned in Ref. [19], but was not discussed further. However, when the incident LG beam deviates from the center of the astigmatism phase, the converted HG beam does not appear at the corresponding position on the output plane, which can cause confusion in applications.

Ao Tang and Guangyun Xiong are with the Key Laboratory on Adaptive Optics, Chinese Academy of Science, Institute of Optics and Electronics, Chinese Academy of Science, Chengdu 610209, China, and also with the University of Chinese Academy of Sciences, Beijing 100049, China (e-mail: tangao18@mails.ucas.ac.cn; xiongguangyun20@mails.ucas.ac.can).

Lan Bin and Feng Shen are with the Key Laboratory on Adaptive Optics, Chinese Academy of Science, Institute of Optics and Electronics, Chinese Academy of Science, Chengdu 610209, China (e-mail: lanbin@ioe.ac.cn; shenfeng@ioe.ac.cn).

In this paper, the spatial mapping relationship between the LG beams array and the HG beams array is theoretically analyzed and experimentally demonstrated. This work theoretically perfects the position correspondence of the interconversion between LG beams and HG beams based on an astigmatism phase, and also provides a theoretical support for measuring the LG beams array.

II. THEORETICAL ANALYSIS

The HG mode can be converted to the LG mode by the following transformation [18].

$$LG_{l,p}(x,y) = \int \int \exp\left[-\mathrm{i}(x\xi + y\eta) + \mathrm{i}\psi(\xi,\eta)\right]$$

$$\times HG_{n,m}\left(\frac{\xi}{\omega},\frac{\eta}{\omega}\right)\mathrm{d}\xi\mathrm{d}\eta, \tag{1}$$

Where, ξ, η are the rectangular coordinates of the input plane, x, y are the rectangular coordinates of the output plane. ψ is an astigmatism phase, the expression is

$$\psi(\xi,\eta) = \alpha[(\xi^2 - \eta^2)\cos 2\theta + 2\xi\eta\sin 2\theta], \tag{2}$$

Where, α is the strength coefficient of the astigmatism phase, θ is the angle of the astigmatism phase. This phase is also employed in image processing [27], [28]. In (1), both the LG mode and HG mode are special solutions of Maxwell's equations [19], and their optical fields can be expressed as follows

$$HG_{n,m}\left(\frac{\xi}{\omega},\frac{\eta}{\omega}\right) = \exp\left(-\frac{\xi^2 + \eta^2}{\omega^2}\right)H_n\left(\frac{\sqrt{2}\xi}{\omega}\right)$$

$$\times H_m\left(\frac{\sqrt{2}\eta}{\omega}\right)$$

$$LG_{l,p}\left(\frac{x}{\omega},\frac{x}{\omega}\right) = \exp\left(-\frac{x^2 + y^2}{\omega^2}\right)\left(\frac{x \pm \mathrm{i}y}{\omega}\right)^l$$

$$\times L_p^l\left(2\frac{x^2 + y^2}{\omega^2}\right), \tag{3}$$

Here, ω is the beam waist, n, m are mode number of the HG beam. l, p are angular index and radial index of the LG beam, respectively. $H(x)$ and $L(x)$ are the Hermite polynomial and the Laguerre polynomial, respectively.

For HG beams that deviate from the astigmatism phase center, it can be expressed as $HG_{n,m}\left(\frac{\xi+X}{\omega},\frac{\eta+Y}{\omega}\right)$. X, Y denote the displacement in horizontal and vertical directions, respectively. According to (1), such an HG beam can be converted as follows

$$F(x,y) = \int \int \exp[-\mathrm{i}(x\xi + y\eta) + \mathrm{i}\psi(\xi,\eta)]$$

$$\cdot HG_{n,m}\left(\frac{\xi+X}{\omega},\frac{\eta+Y}{\omega}\right)\mathrm{d}\xi\mathrm{d}\eta, \tag{4}$$

To simplify (4), converting (ξ,η) in the exponential part of the (4) to $(\xi+X,\eta+Y)$, and following expression can be obtained.

$$F(x,y) = \int \int C_1 C_2 \exp[-\mathrm{i}(x(\xi+X) + y(\eta+Y))$$

$$+ \mathrm{i}\psi((\xi+X),(\eta+Y))]$$

$$\times HG_{n,m}\left(\frac{\xi+X}{\omega},\frac{\eta+Y}{\omega}\right)\mathrm{d}\xi\mathrm{d}\eta, \tag{5}$$

Here, C_1, C_2 as follows

$$C_1 = \exp[\mathrm{i}(xX + yY) + \mathrm{i}a(X^2 - Y^2)\cos 2\theta + \mathrm{i}2aXY\sin 2\theta]$$

$$C_2 = \exp[-\mathrm{i}2a((\xi+X)X - (\eta+Y)Y)\cos 2\theta$$

$$- \mathrm{i}2a((\xi+X)Y + (\eta+Y)X)\sin 2\theta], \tag{6}$$

Where, C_1 is independent of (ξ,η) and can be referred to outside the integral. Substituting (6) into (5), and the differential $\mathrm{d}\xi\mathrm{d}\eta$ in (5) can be transformed to $\mathrm{d}(\xi+X)\mathrm{d}(\eta+Y)$, then, letting (ξ,η) replace $(\xi+X,\eta+Y)$, the following expression can be given out.

$$F(x,y,a,\theta) = C_1 \int \int \exp[-\mathrm{i}(x\xi + y\eta)$$

$$+ \mathrm{i}\psi(\xi,\eta,a,\theta)]$$

$$\times HG_{n,m}\left(\frac{\xi}{\omega},\frac{\eta}{\omega}\right)\cdot\exp[-\mathrm{i}2a(\xi X - \eta Y)$$

$$\times \cos 2\theta - \mathrm{i}2a(\xi Y + \eta X)\sin 2\theta]\mathrm{d}\xi\mathrm{d}\eta, \tag{7}$$

In (7), $HG_{n,m}\left(\frac{\xi}{\omega},\frac{\eta}{\omega}\right)$ can be simplified as [19]

$$\sum_{n,m=0}^{\infty} HG_{n,m}\left(\frac{\xi}{\omega},\frac{\eta}{\omega}\right) \times \frac{s^n}{n!}\frac{t^n}{m!}$$

$$= \exp\left(-\frac{\xi^2 + \eta^2}{\omega^2}\right)\cdot\exp\left(-s^2 + 2\frac{\sqrt{2}\xi}{\omega}s\right)$$

$$\times \exp\left(-t^2 + 2\frac{\sqrt{2}\eta}{\omega}t\right), \tag{8}$$

Substituting (8) and (2) into (7), the following expression can be derived.

$$\sum_{n,m=0}^{\infty} F(x,y) \times \frac{s^n}{n!}\frac{t^n}{m!} = C_1 \times \exp(-s^2 - t^2)$$

$$\times \int \int \exp\left(-\mathrm{i}\begin{bmatrix}x\\y\end{bmatrix}\cdot\begin{bmatrix}\xi\\\eta\end{bmatrix} + \frac{2\sqrt{2}}{\omega}\begin{bmatrix}s\\t\end{bmatrix}\cdot\begin{bmatrix}\xi\\\eta\end{bmatrix}\right.$$

$$+ \left[\begin{matrix}\frac{1}{\omega^2} - \mathrm{i}\alpha\cos 2\theta & -\mathrm{i}\alpha\sin 2\theta \\ -\mathrm{i}\alpha\sin 2\theta & \frac{1}{\omega^2} + \mathrm{i}\alpha\cos 2\theta\end{matrix}\right]\otimes\begin{bmatrix}\xi\\\eta\end{bmatrix}\cdot\begin{bmatrix}\xi\\\eta\end{bmatrix}\right)$$

$$\times \exp\left(2\alpha\mathrm{i}\begin{bmatrix}-X & -Y\\Y & -X\end{bmatrix}\otimes\begin{bmatrix}\cos 2\theta\\\sin 2\theta\end{bmatrix}\cdot\begin{bmatrix}\xi\\\eta\end{bmatrix}\right)\mathrm{d}\xi\mathrm{d}\eta$$

$$= C_1 \times \exp(-s^2 - t^2)\int\int \exp\left[\langle\boldsymbol{\tau},\boldsymbol{\zeta}\rangle\right.$$

$$- \langle\boldsymbol{A}\boldsymbol{\zeta},\boldsymbol{\zeta}\rangle + 2\alpha\mathrm{i}\langle\boldsymbol{FT},\boldsymbol{\zeta}\rangle]\mathrm{d}\boldsymbol{\zeta}$$

$$= C_1 \times \exp(-s^2 - t^2)\int\int \exp\left[\langle\boldsymbol{\Theta},\boldsymbol{\zeta}\rangle - \langle\boldsymbol{A}\boldsymbol{\zeta},\boldsymbol{\zeta}\rangle\right]\mathrm{d}\boldsymbol{\zeta}, \tag{9}$$

Where, "·" and "⟨⟩" represent the inner product of vectors, and "⊗" denotes the vector outer product. A, τ, ζ, F, T represent as follows

$$A = \begin{bmatrix} \frac{1}{\omega^2} - i\alpha\cos 2\theta & -i\alpha\sin 2\theta \\ -i\alpha\sin 2\theta & \frac{1}{\omega^2} + i\alpha\cos 2\theta \end{bmatrix}, \quad \tau = \begin{bmatrix} \frac{2\sqrt{2}s}{\omega} - ix \\ \frac{2\sqrt{2}t}{\omega} - iy \end{bmatrix}$$

$$\zeta = \begin{bmatrix} \xi \\ \eta \end{bmatrix}, \quad F = \begin{bmatrix} -X & -Y \\ Y & -X \end{bmatrix}, \quad T = \begin{bmatrix} \cos 2\theta \\ \sin 2\theta \end{bmatrix}, \quad (10)$$

And in (9), $\Theta = \tau + 2\alpha i FT$, the following expression can be obtained after expansion.

$$\Theta = \begin{bmatrix} 2\frac{\sqrt{2}s}{\omega} - i\,[x + 2\alpha\,(X\cos 2\theta + Y\sin 2\theta)] \\ 2\frac{\sqrt{2}t}{\omega} - i\,[y + 2\alpha\,(-Y\cos 2\theta + X\sin 2\theta)] \end{bmatrix}, \quad (11)$$

According to Ref. [29], $\int \ldots N \ldots \int \exp(-\langle x, Ax \rangle) dx = \frac{\pi^{N/2}}{\sqrt{|A|}}$, (9) can be simplified as

$$\sum_{n,m=0}^{\infty} F(x,y) \times \frac{s^n}{n!}\frac{t^n}{m!}$$

$$= \frac{\pi}{\sqrt{|A|}} C_1 \exp\left(-s^2 - t^2 + \frac{1}{4}\langle A^{-1}\Theta, \Theta \rangle\right)$$

$$F(x,y) = \frac{\pi}{\sqrt{|A|}} C_1 \frac{\partial^{n+m}}{\partial s^n \partial t^n}$$

$$\times \exp\left(-s^2 - t^2 + \frac{1}{4}\langle A^{-1}\Theta, \Theta \rangle\right)\Big|_{s=t=0}, \quad (12)$$

Where, $\alpha = \frac{1}{\omega^2}$. According on the derivation in Ref. [19], and substituting into the expression C_1 in (6), it follows that

$$F(x,y) = \frac{\pi\omega^2}{\sqrt{2}}(-1)^{n+m}\exp\left(-i\frac{\omega^2 x_1 y_1}{4}\right)$$

$$\times \begin{cases} (2i)^n m! LG_{m,n-m}\left(\frac{\omega x_1}{2\sqrt{2}}, \frac{\omega y_1}{2\sqrt{2}}\right), & n \geq m \\ (2i)^m n! LG_{n,m-n}\left(\frac{\omega x_1}{2\sqrt{2}}, \frac{\omega y_1}{2\sqrt{2}}\right), & n \leq m \end{cases}, \quad (13)$$

Where, $x_1 = x + 2(X\cos 2\theta + Y\sin 2\theta)/\omega^2$, $y_1 = y + 2(-Y\cos 2\theta + X\sin 2\theta)/\omega^2$. Since the transformation of (1) is invertible, and the inverse transformation of (13) can be derived

$$HG_{n,m}\left(\frac{x_1}{\omega}, \frac{y_1}{\omega}\right) = \int\int \exp[-i(x\xi + y\eta) + i\psi(\xi,\eta)]$$

$$LG_{l,p}(\xi + X, \eta + Y)d\xi d\eta, \quad (14)$$

From (14), when incident LG beam is deviated from the astigmatism phase center, the converted HG beam can also be deviated from the center, and the magnitude and direction of the displacement are determined by the angle θ of the astigmatism phase. Here, four common angles are chosen for the analysis, as shown in Table I. From Table I, employing 0° or 90° astigmatism phase, the positions of the LG and HG beams are symmetric about x axis or y axis. Additionally, employing 45° or −45° astigmatism phase, the positions of the LG and HG beams are symmetric about $y = x$ or $y = -x$. This is a very interesting

TABLE I
THE MAPPING RELATIONSHIP BETWEEN LG BEAM AND HG BEAM AT DIFFERENT ANGLES OF ASTIGMATISM PHASE

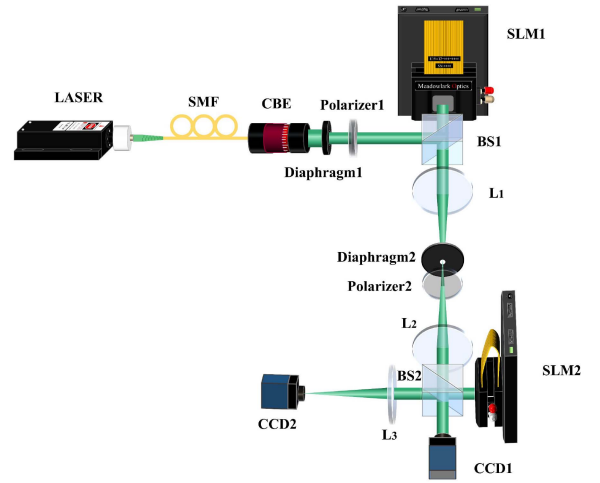| Angle (θ)	Phase	Displacement		Axis of symmetry
		LG beam	HG beam	
0°	$\frac{2(\xi^2 + \eta^2)}{\omega^2}$	$(\xi + X, \eta + Y)$	$\left(x + \frac{2}{\omega^2}X, y - \frac{2}{\omega^2}Y\right)$	x axis
90°	$-\frac{2(\xi^2 + \eta^2)}{\omega^2}$	$(\xi + X, \eta + Y)$	$\left(x - \frac{2}{\omega^2}X, y + \frac{2}{\omega^2}Y\right)$	y axis
45°	$\frac{2\xi\eta}{\omega^2}$	$(\xi + X, \eta + Y)$	$\left(x + \frac{2}{\omega^2}Y, y + \frac{2}{\omega^2}X\right)$	$y=x$
-45°	$-\frac{2\xi\eta}{\omega^2}$	$(\xi + X, \eta + Y)$	$\left(x - \frac{2}{\omega^2}Y, y - \frac{2}{\omega^2}X\right)$	$y=-x$

Fig. 1. Experimental setup for generating and measuring LG beams array.

discovery. Furthermore, the l information of each LG beam in the LG beams array can be obtained by measuring the HG beam at the corresponding position.

III. EXPERIMENTAL SETUP AND RESULTS

The experimental results of the interconversion between LG and HG beams with the astigmatism phase are well known [30], therefore, in this paper, the LG beams arrays with radial index $p = 0$ are only generated to verify the above derived theories. A spatial light modulator (SLM) is usually used to generate the LG beams [31]. Here, the complex amplitude modulation technology [32] is employed to generate LG beams arrays. The experimental setup as shown in Fig. 1. In the experiment, a 532 nm laser with single-mode fiber (SMF) coupling output is employed. The beam emitted is collimated and expanded by employed a collimated beam expander (CBE). Then, the beam size is controlled by utilizing an adjustable diaphragm 1 to fit the active area of the SLM1, and the polarization state of the beam is adjusted by employed the rotatable polarizer 1 to conform to the polarization state of the SLM1. The phase-only SLM1 (1920 × 1200 pixels, 8 um per pixel) is utilized to generate the LG beams array, after the beam is reflected by the beam splitting prism 1
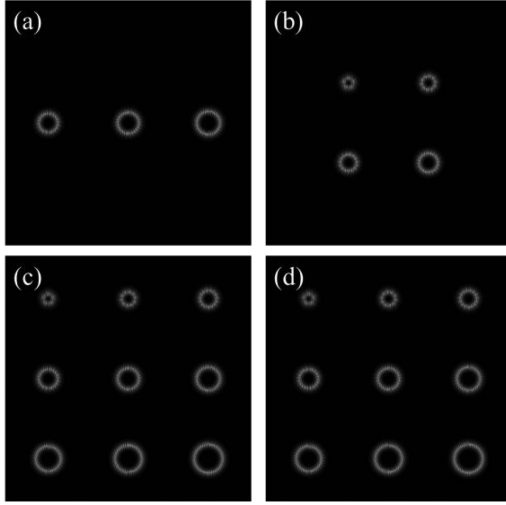
Fig. 2. The phase patterns loaded into SLM1 for generating the LG beams array, (a) 1×3, (b) 2×2, (c) 3×3 with same sign, (d) 3×3 with different sign.

Fig. 3. The LG beam arrays with different dimensions detected by the CCD1, (a) 1×3, (b) 2×2, (c) 3×3 with same sign, (d) 3×3 with different sign.

(BS1). The phase pattern loaded into the SLM1 is superimposed with a blazed grating to separate the target light field from the zero-level diffraction. For the convenience of observing the generated LG beams array, a 4f system is built, consisting of lens L_1 and lens L_2, with focal lengths of $f_1 = 150$ mm and $f_2 = 150$ mm, respectively. An adjustable diaphragm 2 is placed at the focal plane of the lens L_1 to remove other diffraction orders and obtain only first-order diffraction. Then, the generated LG beams array is recorded by CCD1. The generated LG beams array is reflected by BS2, and illuminates on the active area of SLM2, which is employed to load the astigmatism phase with different angle to convert the LG beams array into HG beams array. The distance from BS2 to SLM2 is equal to the distance from BS2 to CCD1, ensuring that SLM2 is on the focal plane of lens L_2. Then, the lens L_3, $f_3 = 150$ mm, is utilized to obtain far-field optical field, and the converted HG beams array is recorded by CCD2.

According to the type 3 computer-generated hologram of Ref. [32], the phase patterns used for generating LG beams array are obtained, as shown in Fig. 2, and load into SLM1. Then, LG beams arrays with different dimensions are detected by CDD1, as shown in Fig. 3. Fig. 3(a) displays 1×3 LG beams array, from left to right, the l are -4, 5, -6. Fig. 3(b) is 2×2 LG beams array, the l are 1, -2, 3, -4 sequentially. Fig. 3(c) and (d) represent 3×3 LG beams arrays with same sign l and with different sign l, and the absolute values of the l are from 1 to 9, as denoted by the white numbers in Fig. 3(c) and (d).

Next, the generated LG beams arrays is converted to HG beams arrays using the astigmatism phases. Fig. 4 shows the different angle astigmatism phases loaded to SLM2. Fig 4(a) and (b) are $\theta = 0°$ and $\theta = 90°$, respectively. Fig 4(c) and (d) are $\theta = 45°$ and $\theta = -45°$, respectively. From Fig. 4, the angle in (2) has no effect on the astigmatism phase, but only plays a rotational role.

Fig. 5 displays the experimental results of converting LG beams arrays in Fig. 3 to HG beams arrays at different angle
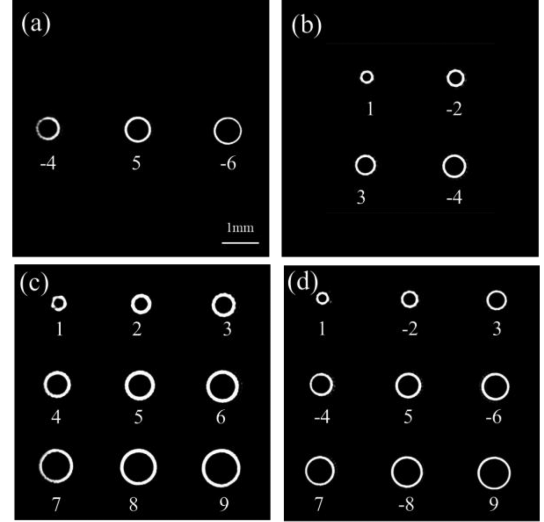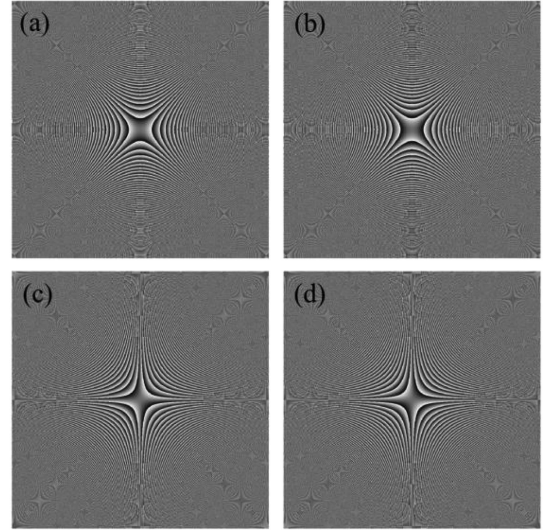

Fig. 4. The astigmatism phase with different angle loaded into SLM2, (a) $\theta = 0°$, (b) $\theta = 90°$, (c) $\theta = 45°$, (d) $\theta = -45°$.

astigmatism phases. Fig. 5(a)–(d) employ an astigmatism phase with $\theta = 0°$, and Fig. 5(a1)–(d1) use an astigmatism phase with $\theta = 90°$. From Fig. 5(c) and (c1), for the LG beams with same sign, the direction of the converted HG beam with 0° astigmatism phase is $-45°$, and the direction of the HG beam obtained by 90° astigmatism phase is 45°. From Fig. 4, the 90° astigmatism phase is based on the 0° astigmatism phase rotated by 90°. Therefore. for the LG beam with same sign, the HG beams converted by these two astigmatism phase are perpendicular each other. For the LG beams with different sign, the HG beams converted by same astigmatism phase are also perpendicular each other, as shown in Fig. 5(d) and (d1). The OAM state of LG beam can be easily judged from the field distribution of the converted HG beam, in which the dark fringes number between at bright spots both ends reveals the magnitude of the l, and the fringe orientation reveals the sign of the l.
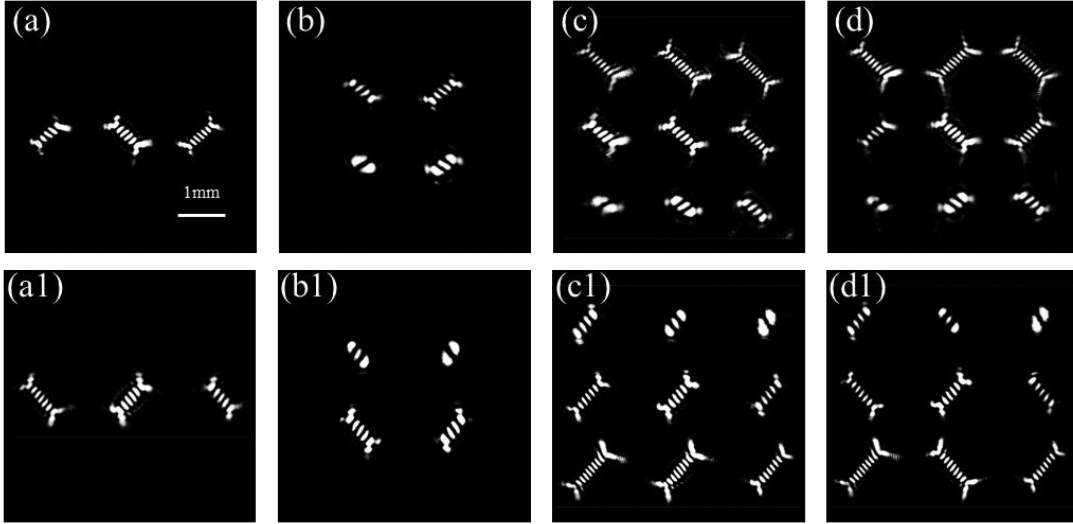
Fig. 5. The experimental results of converting LG beams array in Fig. 3 to HG beams array at different angle astigmatism phases, (a)–(d) $\theta = 0°$, (a1)–(d1) $\theta = 90°$.

TABLE II
THE l MATRIX OF THE INCIDENT LG BEAMS ARRAY AND THE l MATRIX OBTAINED FROM THE CONVERTED HG BEAMS ARRAY

Incident LG beams array	Converted HG beams array			
	Fig. 5 (a), (b), (d)	Fig. 5 (a1), (b1), (d1)	Fig. 6 (a), (b), (d)	Fig. 6 (a1), (b1), (d1)
$\begin{bmatrix} -4 & 5 & -6 \end{bmatrix}$	$\begin{bmatrix} -4 & 5 & -6 \end{bmatrix}$	$\begin{bmatrix} -6 & 5 & -4 \end{bmatrix}$	$\begin{bmatrix} -6 \\ 5 \\ -4 \end{bmatrix}$	$\begin{bmatrix} -4 \\ 5 \\ -6 \end{bmatrix}$
$\begin{bmatrix} 1 & -2 \\ 3 & -4 \end{bmatrix}$	$\begin{bmatrix} 3 & -4 \\ 1 & -2 \end{bmatrix}$	$\begin{bmatrix} -2 & 1 \\ -4 & 3 \end{bmatrix}$	$\begin{bmatrix} -4 & -2 \\ 3 & 1 \end{bmatrix}$	$\begin{bmatrix} 1 & 3 \\ -2 & -4 \end{bmatrix}$
$\begin{bmatrix} 1 & -2 & 3 \\ -4 & 5 & -6 \\ 7 & -8 & 9 \end{bmatrix}$	$\begin{bmatrix} 7 & -8 & 9 \\ -4 & 5 & -6 \\ 1 & -2 & 3 \end{bmatrix}$	$\begin{bmatrix} 3 & -2 & 1 \\ -6 & 5 & -4 \\ 9 & -8 & 7 \end{bmatrix}$	$\begin{bmatrix} 9 & -6 & 3 \\ -8 & 5 & -2 \\ 7 & -4 & 1 \end{bmatrix}$	$\begin{bmatrix} 1 & -4 & 7 \\ -2 & 5 & -8 \\ 3 & -6 & 9 \end{bmatrix}$

The first column of Table II illustrates the l matrices of incident LG beams arrays for Fig. 3(a), (b) and (d). The second column of Table II displays measured l matrices for Fig. 5(a), (b) and (d). According to Tables I and II, the experimental results are good consistent the theoretical analysis, and the l matrices obtained are turned up and down about the x axis. In Fig. 5(a), as the array is one-dimensional in the horizontal direction, the measurement results remain constant.

The third column of Table II is the experimental results for Fig. 5(a1), (b1) and (d1). The obtained l matrices are turned left and right about the y axis, compared to the l matrices on the incident plane, which is completely consistent with the above theoretical analysis.

Fig. 6(a)–(d) and (a1)–(d1) display the converted HG beams arrays at $\theta = 45°$ and $\theta = -45°$ astigmatism phases, respectively. Different from Fig. 5, for the LG beam with the positive l, the direction of the converted HG beam in Fig. 6(c) is horizontal,

and the converted HG beam in Fig. 6(c1) is in the vertical. However, for the LG beam with the negative l, the direction of the converted HG beam is reversed. These is related to the angle of the astigmatism phase.

The fourth column of Table II is experimental results for Fig. 6(a), (b) and (d), compared to incident LG beams arrays, the obtained l matrices are turned over about $y = x$, which is completely consistent with the above theoretical analysis.

The experimental results for Fig. 6(a1)–(d1) as shown in the fifth column of Table II. It is obvious that, compared to incident LG beams array, the obtained l matrices are turned over about the $y = -x$, which is completely consistent with the above theoretical analysis. This relationship can also be considered as matrix transpose.

According to the above derived position mapping relationship, the l matrix obtained from the converted HG beams array
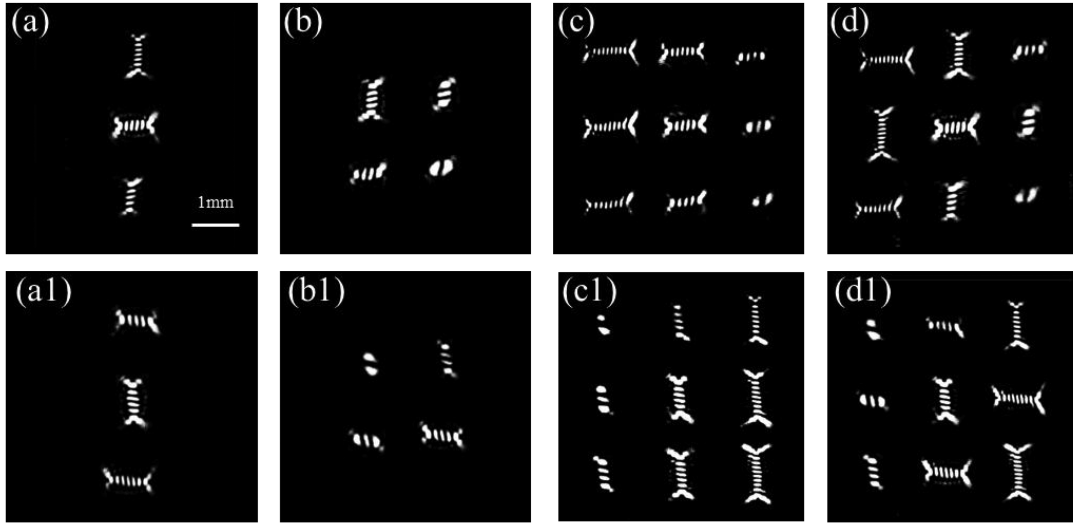
Fig. 6.   The experimental results of converting LG beams array in Fig. 3 to HG beams array at different angle astigmatism phases, (a)–(d) $\theta = 45°$, (a1)–(d1) $\theta = -45°$.

is done with the corresponding position transformation, and correct l information of LG beams array is derived.

IV. DISCUSSION

From the above experimental results, the incident LG beam that deviates from the phase center, the converted HG beam is not distorted. As a result, although only experiments for 3×3 LG beams arrays are conducted in this paper, this method can theoretically measure infinite dimensional LG beams array as long as the astigmatism phase is large enough. Additionally, the maximum l measured in this paper reach only 9, however, LG beams up to 100th order can be measured using an astigmatism phase, which has been analyzed in detail in Ref. [22]. Moreover, no crosstalk of adjacent HG modes using this method, as the beam size of LG beams increases with the l, and its amplitude characteristics have been discussed in detail in Ref. [33], then, converted HG beam can be accommodated in its corresponding space. Furthermore, the size of the converted HG beam can be adjusted by changing the focal length of the lens to obtain a appropriate fringe resolution. Consequently, for high-order, arbitrary-dimensional LG beams arrays, this method can still be employed for measurements.

V. CONCLUSION

In this paper, based on the single beam, the interconversion of LG beams array and HG beams array with the astigmatism phase is investigated and the spatial mapping relationship is derived. Furthermore, based on this theory, theoretically, high-order, arbitrary-dimensional LG beams arrays can be measured as long as the astigmatism phase is enough, which is simple and efficient. This work theoretically perfects the position correspondence of the interconversion of LG beams and HG beams based on an astigmatism phase, and has promising applications for multi-channel OAM communications and optical tweezers.

REFERENCES

[1] L. Allen, M. W. Beijersbergen, R. J. C. Spreeuw, and J. P. Woerdman, "Orbital angular momentum of light and the transformation of Laguerre-Gaussian laser modes," *Phys. Rev. A*, vol. 45, no. 11, pp. 8185–8189, 1992.

[2] G. Gibson et al., "Free-space information transfer using light beams carrying orbital angular momentum," *Opt. Exp.*, vol. 12, no. 22, pp. 5448–5456, 2004.

[3] Z. Wan, Y. Shen, Z. Wang, Z. Shi, Q. Liu, and X. Fu, "Divergence-degenerate spatial multiplexing towards future ultrahigh capacity, low error-rate optical communications," *Light: Sci. Appl.*, vol. 11, no. 1, pp. 1–11, 2022.

[4] X. Ouyang et al., "Synthetic helical dichroism for six-dimensional optical orbital angular momentum multiplexing," *Nature Photon.*, vol. 15, no. 12, pp. 901–907, 2021.

[5] M. Padgett and R. Bowman, "Tweezers with a twist," *Nature Photon.*, vol. 5, no. 6, pp. 343–348, 2011.

[6] J. Ni, C. Wang, C. Zhang, Y. Hu, L. Yang, and Z. Lao, "Three-dimensional chiral microstructures fabricated by structured opticalvortices in isotropic material," *Light: Sci. Appl.*, vol. 6, no. 7, 2017, Art. no. e17011.

[7] J. Leach, M. J. Padgett, S. M. Barnett, S. Franke-Arnold, and J. Courtial, "Measuring the orbital angular momentum of a single photon," *Phys. Rev. Lett.*, vol. 88, no. 25, 2002, Art. no. 257901.

[8] S. Cui et al., "Determining topological charge based on an improved Fizeau interferometer," *Opt. Exp.*, vol. 27, no. 9, pp. 12774–12779, 2019.

[9] S. Zhang, P. Li, and S. Wang, "Ultrafast vortices generation at low pump power and shearing interferometer-based vortex topological detection," *Laser Phys. Lett.*, vol. 16, no. 3, 2019, Art. no. 035302.

[10] P. Kumar and N. K. Nishchal, "Self-referenced spiral interferogram using modified lateral shearing Mach–Zehnder interferometer," *Appl. Opt.*, vol. 58, no. 25, pp. 6827–6833, 2019.

[11] J. M. Hickmann, E. J. S. Fonseca, W. C. Soares, and S. Chávez-Cerda, "Unveiling a truncated optical lattice associated with a triangular aperture using light's orbital angular momentum," *Phys. Rev. Let.*, vol. 105, no. 5, 2010, Art. no. 053904.

[12] S. M. A. Hosseini-Saber, E. A. Akhlaghi, and A. Saber, "Diffractometry-based vortex beams fractional topological charge measurement," *Opt. Lett.*, vol. 45, no. 13, pp. 3478–3481, 2020.

[13] H. Gao et al., "Topological charge measurement of concentric OAM states using the phase-shift method," *J. Opt. Soc. Amer. A*, vol. 35, no. 1, pp. A40–A44, 2018.

[14] X. Wang et al., "Learning to recognize misaligned hyperfine orbital angular momentum modes," *Photon. Res.*, vol. 9, no. 4, pp. B81–B86, 2021.

[15] Y. Guo et al., "Spin-decoupled metasurface for simultaneous detection of spin and orbital angular momenta via momentum transformation," *Light: Sci. Appl.*, vol. 10, no. 1, pp. 1–12, 2021.

[16] A. D'Errico et al., "Measuring the complex orbital angular momentum spectrum and spatial mode decomposition of structured light beams," *Optica*, vol. 4, no. 11, pp. 1350–1357, 2017.

[17] Y. Wang, L. Bai, D. Zhang, J. Xie, Y. Guo, and L. Guo, "Spiral spectrum of a Laguerre-Gaussian beam propagating in anisotropic turbulent plasma," *IEEE Photon. J.*, vol. 13, no. 6, Dec. 2021, Art. no. 7900310.

[18] H. Zhou et al., "Measuring the orbital angular momentum state of light by coordinate transformation," *IEEE Photon. Technol. Lett.*, vol. 29, no. 1, pp. 86–89, Jan. 2017.

[19] E. Abramochkin and V. Volostnikov, "Beam transformations and nontransformed beams," *Opt. Commun.*, vol. 83, no. 1-2, pp. 123–135, 1991.

[20] G. Liang and Q. Wang, "Power steered modes conversions and rotations in nonlocal nonlinear media," *J. Opt.*, vol. 21, no. 12, 2019, Art. no. 125504.

[21] G. Liang and Q. Wang, "Controllable conversion between Hermite Gaussian and Laguerre Gaussian modes due to cross phase," *Opt. Exp.*, vol. 27, no. 8, pp. 10684–10691, 2019.

[22] Z. Liu, S. Gao, and W. Xiao, "Measuring high-order optical orbital angular momentum with a hyperbolic gradually changing period pure-phase grating," *Opt. Lett.*, vol. 43, no. 13, pp. 3076–3079, 2018.

[23] Y. Wu, H. Liu, and X. Chen, "Highly efficient detection of near-infrared optical vortex modes with frequency upconversion," *Opt. Lett.*, vol. 47, no. 10, pp. 2474–2477, 2022.

[24] Y. Yang, L. Niu, Z. Yang, and J. Liu, "Measuring the topological charge of terahertz vortex beams with a focal hyperbolic lens," *Appl. Opt.*, vol. 59, no. 15, pp. 4685–4691, 2020.

[25] M. Piccardo et al., "Vortex laser arrays with topological charge control and self-healing of defects," *Nature Photon.*, vol. 16, no. 5, pp. 359–365, 2022.

[26] S. Zheng and J. Wang, "Measuring orbital angular momentum (OAM) states of vortex beams with annular gratings," *Sci. Rep.*, vol. 7, no. 1, pp. 1–9, 2017.

[27] J. A. Rodrigo, T. Alieva, and M. L. Calvo, "Gyrator transform: Properties and applications," *Opt. Exp.*, vol. 15, no. 5, pp. 2190–2203, 2007.

[28] Z. Liu et al., "Fast algorithm of discrete gyrator transform based on convolution operation," *Optik*, vol. 122, no. 10, pp. 864–867, 2011.

[29] R. Bellman, "Functions of matrices," in *Introduction to Matrix Analysis*, 2nd ed., New York, NY, USA: Society for Industrial and Applied Mathematics, 1997, pp. 97–98.

[30] D. Shen, T. He, X. Yu, and D. Zhao, "Mode conversion and transfer of orbital angular momentum between Hermite-Gaussian and Laguerre-Gaussian beams," *IEEE Photon. J.*, vol. 14, no. 1, Feb. 2022, Art. no. 6510506.

[31] Z. Liu, J. Dai, and X. Sun, "Generation of hollow Gaussian beam by phase-only filtering," *Opt. Exp.*, vol. 16, no. 24, pp. 19926–19933, 2008.

[32] V. Arrizón, U. Ruiz, R. Carrada, and L. A. González, "Pixelated phase computer holograms for the accurate encoding of scalar complex fields," *J. Opt. Soc. Amer. A*, vol. 24, no. 11, pp. 3500–3507, 2007.

[33] A. Tang, L. Bin, G. Xiong, and F. Shen, "Completely revealing the amplitude properties of Laguerre-Gaussian vortex beams," *Opt. Exp.*, vol. 30, no. 16, pp. 28892–28904, 2022.